Linewidth Rebroadening in Quantum Dot Semiconductor Lasers

Christoph Redlich, Benjamin Lingnau, Heming Huang, Ravi Raghunathan, Kevin Schires, Philip Poole, Frédéric Grillot, and Kathy Lüdge

***Abstract*—We investigate the interplay between linewidth and α-factor in quantum dot lasers using experimental data and a minimal quantum dot laser rate equation model. The rebroadening of the laser linewidth found experimentally at high injection currents is explained by analytical means and traced back to nonlinear scattering processes. Important differences of the pump current dependent linewidth evolution of quantum dot lasers are highlighted especially if compared to conventional laser devices. Furthermore, we provide a scheme to extract the amplitude-phase coupling as well as effective carrier scattering rates with standard characterization techniques, i.e., linewidth, light versus injected pump current and modulation response measurements.**

***Index Terms*—Semiconductor lasers, quantum well lasers, nonlinear optics, nonlinear dynamical systems, photonics.**

I. Introduction

SEMICONDUCTOR lasers with quantum dots (QDs) as the active material have been of deep interest in the last decades [1], [2]. With their highly confined carriers, i.e. their atom-like electronic structure, they have shown many interesting properties, such as very low bias currents, high modulation bandwidths, temperature insensitivity. Compared to bulk or quantum-well (QW) lasers, the self-organized grown QD lasers consist of differently sized quantum dots, consequently leading to an inhomogeneously broadened gain spectrum [3]. Due to the dynamical coupling of the charge carriers to the reservoir states, quantum dot lasers offer very rich dynamical properties [4]. In this sense, the laser linewidth can be seen as the dynamical answer of the quantum dot laser to spontaneous emission noise, therefore characterizing the dynamic response to optical perturbations. Here, the amplitude-phase coupling, often referred as α or Henry-factor, is of particular importance as it measures the connection between refractive index shift and the carrier density changes in the gain medium [5]. For quantum-well lasers, it is well known that the refractive index and the gain show a linear dependence, leading to a constant α-factor[6] and an enhancement of the optical laser linewidth [7]. For quantum-dot lasers the situation is more involved [8]–[11] and standard techniques as, e.g., FM/AM techniques, are not suitable to derive a single value for the α-factor [12]–[14] or properly describe the phase noise of a QD laser [15]. In the following, we investigate the rebroadening of the laser linewidth that was found in QD lasers within a semi-classical theory. In the literature, one already finds QD rate equation models that capture linewidth rebroadening and show an analytic formula for α [10]. Their findings are included within our theory for special parameters.

Based on a minimal variable rate-equation QD laser model, we find a (semi-)analytical formula for the laser linewidth and the corresponding α-factor. In contrast to former research, the minimal model not only describes the phase fluctuations and linewidth properties of the QD laser, but also investigates the effect of gain compression on the rebroadening of the laser linewidth. In comparison to existing minimal QD laser models[10], [16], we explicitly include scattering processes allowing the escape of charge carriers from the QDs. The quasi-equilibrium QD occupation is then given by the detailed balance of in and out-scattering processes, which we show to play an important role in the calculation of the laser linewidth. The charge carrier dynamics are also important for the performance of the QD laser under current modulation [17]–[19]. An analytic formula for the modulation response is derived and its dependence on the injection current is shown. All results, including the light vs injected pump current (LI)-curve, are backed by our experimental findings and give insight into the tight connection of the charge carrier scattering rates, charge carrier dynamics and the linewidth. Finally, we sketch a method to extract information about the scattering rates and the dynamic amplitude phase coupling with easily accessible measurements.

Manuscript received February 8, 2017; revised April 11, 2017; accepted April 27, 2017. This work was supported in part by the DFG within the GRK 1558 and in part by the DAAD within the PROCOPE Project 57050013. The work of R. Raghunathan was supported by the 2014 "Research in Paris" fellowship awarded by the Mairie de Paris. The work of K. Lüdge was supported by the Humboldt Foundation in the framework of a Feodor Lynen Scholarship for Experienced Researchers. *(Corresponding author: Christoph Redlich.)*

C. Redlich and B. Lingnau are with the Institut für Theoretische Physik, Technische Universität Berlin, Berlin 10623 Germany (e-mail: redlich@tu-berlin.de; lingnau@mailbox.tu-berlin.de)

H. Huang, R. Raghunathan, and K. Schires are with the Télécom ParisTech, Université Paris-Saclay, Paris 75013 France (e-mail: heming.huang@telecom-paristech.fr; ravi.raghunathan@telecom-paristech.fr; kevin.schires@telecom-paristech.fr)

P. Poole is with the National Research Council Canada, Ottawa, ON K1A 0R6 Canada (e-mail: philip.poole@nrc-cnrc.gc.ca)

F. Grillot is with the the Télécom ParisTech, Université Paris-Saclay, Paris 75013 France, and also with the Center for High Technology Materials, University of New-Mexico, Albuquerque, NM 87131 USA (e-mail: frederic.grillot@telecom-paristech.fr)

K. Lüdge is with the Institut für Theoretische Physik, Technische Universität Berlin, Berlin 10623 Germany, and also with the Department of Physics, University of Auckland, Auckland 1010 New Zealand (e-mail: kathy.luedge@tu-berlin.de)

Color versions of one or more of the figures in this paper are available online at http://ieeexplore.ieee.org.

Digital Object Identifier 10.1109/JSTQE.2017.2701555

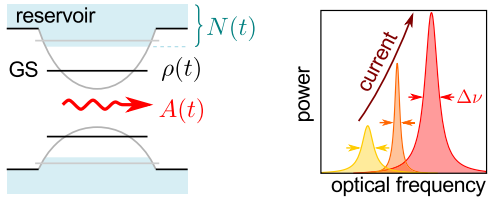

Fig. 1. (a) Sketch of the reduced QD laser model used in this work. The QD ground state is described by its occupation probability $\rho(t)$, the excited and QW states are combined into a single reservoir charge carrier density $N(t)$. The laser field $A(t)$ couples to the QD ground state. (b) Sketch of the optical QD laser spectra showing linewidth rebroadening. With increasing current above the laser threshold, the laser linewidth reaches a minimum for moderate currents (orange), before starting to increase again (red).

II. Semiclassical Single Mode Rate Equation Model

We apply a minimal QD laser model based on our previous works from [19] and exploit the method of adjoint solutions [20] to derive an analytic equation for the laser linewidth. Our model derives from semi-classic theory [21], hence the equations of motion for the carriers are microscopically motivated, whereas the electric field is modeled classically based on Maxwell's equations. Over the last decades the quantum dot laser dynamics was explored on several levels of complexity [22]–[24], however for this investigation a reduced approach derived in [19] is used, as sketched in Fig. 1(a). This approach proved to still capture all important features of QD laser dynamics while still allowing for analytic insights. Three dynamical variables are introduced to describe the single mode quantum dot laser, the reservoir carrier charge density N, the quantum dot carrier occupation probability ρ and the complex electric field envelope $E = Ae^{i\phi}$ described by its amplitude A and phase ϕ. The differential equations describing the dynamics of these quantities inside the QD are given by (1a)–(1d) with stochastic noise sources $P_A(t)$ and $P_\phi(t)$.

$$\dot{N} = J - \frac{N}{T_1} - R\left[\rho^{eq} - \rho\right] \tag{1a}$$

$$\dot{\rho} = R\left[\rho^{eq} - \rho\right] - \frac{\rho}{T_{sp}} - 2g(A)(2\rho - 1)A^2 \tag{1b}$$

$$\dot{A} = g(A)\,(2\rho - 1)A - \kappa A + P_A(t) \tag{1c}$$

$$\dot{\phi} = -g(A)\,(2\rho - 1)\alpha_0 - \delta\Omega N + P_\phi(t) \tag{1d}$$

In this model, the units of $S \equiv A^2 = |E|^2$ and N are non-dimensionalized. We normalize these values to the QD density, such that N, A^2 describe the reservoir charge carrier density and photon density in units of twice the QD density with a factor of 2 for spin degeneracy. ρ is the QD occupation probability for an exciton in the ground state. We include gain compression of the form

$$g(A) = \frac{g_0}{1 + \epsilon A^2} = \frac{g_0}{1 + \epsilon |E|^2} \tag{2}$$

such that the gain is a function of the photon density in the cavity [13], [25], [26]. This term is phenomenologically motivated by our experimental findings (see Fig. 4). The device is electrically pumped with an injection current J, while charge-carrier scattering between the reservoir and the QD states with an effective rate R leads to filling of the quantum dot ground state. The times T_1 and T_{sp} give the carrier lifetimes within the reservoir and the spontaneous emission lifetime of the QD carriers, respectively, while $(2\kappa)^{-1}$ is the photon lifetime.

To derive the scattering contributions, in- and out-scattering rates into and from the quantum dots have to be considered. The number of carriers leaving the quantum dots is proportional to ρ, while the in-scattering only happens with available empty levels and thus proportional to the Pauli blocking factor $(1 - \rho)$. Together both processes define the effective rate $R = R^{\text{in}} + R^{\text{out}}$ that appears in (1a), (1b) and that is defined as $R(\rho^{eq} - \rho) = R^{\text{in}}(1 - \rho) - R^{\text{out}}\rho$. The individual

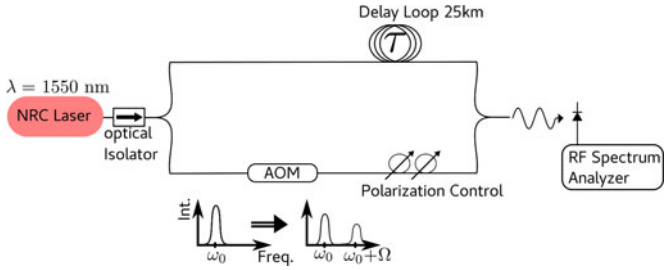

Fig. 2. Experimental setup. A self heterodyne technique was used to obtain the power spectra of the QD laser for injection currents from 45 mA to 180 mA. The distributed feedback laser with InAs dots grown of InP substrate operates at the 1.5 μm telecom wavelength. The optical fibre of the delay loop measures 25 km ($>$100 μs).

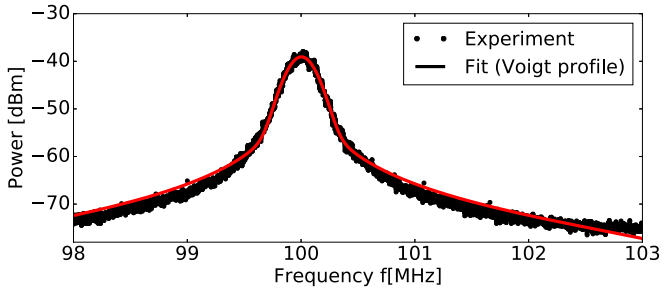

Fig. 3. Experimentally obtained linewidth measurement at an injection current of 60mA. The black dots show the experimental data, while the solid red line shows the fit of a Voigt profile as shown in[44].

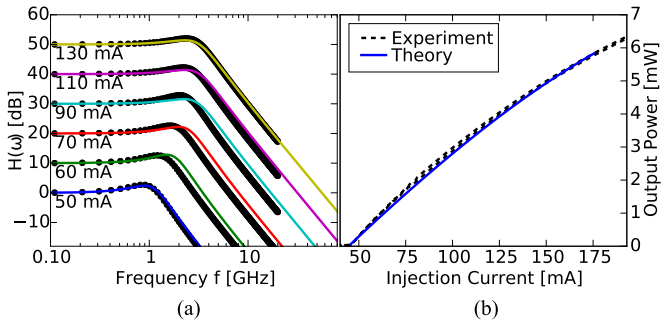

Fig. 4. (a) Measured (dotted) and semi-analytically calculated (solid) modulation response curves of the QD laser versus the injection current modulation frequency in GHz. Different colors indicate different pump currents as labeled in the graph. For readability, we shifted the curves by 10dB each. (b) Measured (solid) and simulated (dotted) LI-curves showing the output power as a function of the injected pump current.

To derive the scattering contributions, in- and out-scattering rates into and from the quantum dots have to be considered. The number of carriers leaving the quantum dots is proportional to ρ, while the in-scattering only happens with available empty levels and thus proportional to the Pauli blocking factor $(1 - \rho)$. Together both processes define the effective rate $R = R^{\text{in}} + R^{\text{out}}$ that appears in (1a), (1b) and that is defined as $R(\rho^{eq} - \rho) = R^{\text{in}}(1 - \rho) - R^{\text{out}}\rho$. The individual

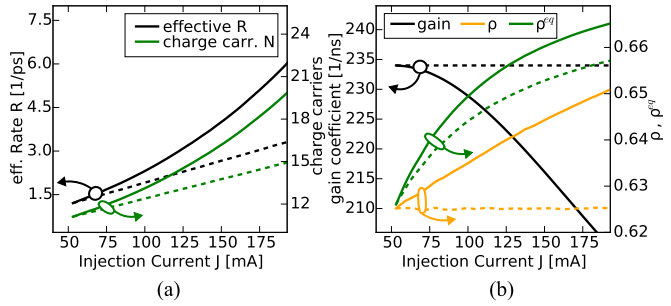

Fig. 5. Numerically obtained steady state values as a function of the pump current: (a) effective scattering rate $R(J)$ and charge carrier density $N(J)$, (b) gain $g(J)$, $\rho(J)$ and $\rho^{eq}(J)$. Results are obtained by solving (1) with parameters gained from fitting the experimental data. Dashed curves represent results without gain compression.

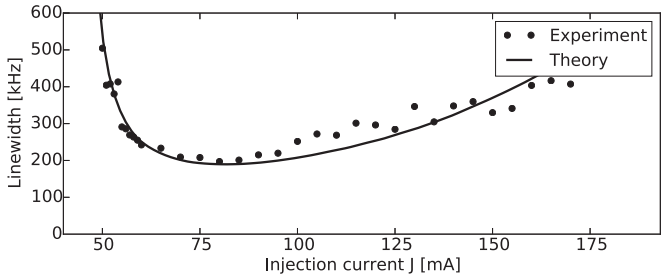

Fig. 6. Measured (symbols) and semianalytically calculated (solid line) linewidth plotted vs the injected pump current. For high injection currents theory and experiment show a rebroadening of the linewidth, with a minimal FWHM of approx. 200 kHz at 75 mA.

rates $R^{\mathrm{in/out}}$ include all possible Coulomb scattering events between the reservoir states and the quantum-dot levels and depend nonlinearly on the carrier density in the reservoir N [27], [28]. Nevertheless, suggested by previous works [9], [29], [30], the connection of the effective scattering rates R and charge carrier density N is almost linear for large carrier densities N, even if multiple scattering processes and relaxations via the QD excited states are considered. We therefore use the linear relation $R(N) = R_{\mathrm{th}} + \frac{\mathrm{d}R}{\mathrm{d}N}|_{\mathrm{th}}(N - N_{\mathrm{th}})$ and $R^{\mathrm{in}}(N) = R^{\mathrm{in}}_{\mathrm{th}} + \frac{\mathrm{d}R^{\mathrm{in}}}{\mathrm{d}N}|_{\mathrm{th}}(N - N_{\mathrm{th}})$ in our minimal model. The occupation $\rho^{eq} = \frac{R^{\mathrm{in}}}{R}$, describes the quasi-equilibrium QD occupation. Note, due to the carrier dependence of the scattering rates, ρ^{eq} dynamically depends on the carrier density in the reservoir.

Variations in the phase of the emitted light are most important for the linewidth of the QD laser. Equation (1d) describes the time derivative of the phase and has to be interpreted with respect to the chosen rotating frame, i.e. the central laser frequency ω_0. Therefore, the phase dynamics $\dot{\phi}$ can be seen as an instantaneous frequency shift $\omega_I = \dot{\phi}$. Noise induced perturbations, described here by the stochastic noise sources $P_A(t)$ and $P_\phi(t)$, change the frequency ω_I and lead to a jitter of the actual laser frequency $\omega_{\mathrm{Laser}} = \omega_0 + \omega_{\mathrm{I}}$. Equation (1d) consists of two terms, each representing one contribution to the frequency shift $\omega_I = \omega_{I,GS} + \omega_{I,ES}$. The first frequency shift is attributed to the carriers in the ground state (GS) of the QDs. Here, the phase is effectively coupled to the real part of the gain $\omega_{\mathrm{I,GS}} = -g(2\rho - 1)\alpha_0$ with a static α-factor α_0, which is often found in QW laser models [26], [31]–[35], and usually named and used in the context of a linear amplitude phase coupling [36]. Note that in these models α_0 emerges from frequency changes due to an index shift caused by off-resonant interband transitions as well as free carrier absorption [37], [38]. In our equations we include these two effects separately, with α_0 denoting the contribution of free carrier absorption involving the QD GS. The stronger contribution from off-resonant interband transitions is modeled by the second term $\omega_{\mathrm{I,ES}} = -\delta\Omega N$, which dynamically depends on the reservoir carrier density N. In our minimal model the charge carrier reservoir N combines both the QD ES and the QW states, treating them as one effective reservoir level. The value of $\delta\Omega$ captures the effect of those levels on the index shift [9].

III. Analytic Description of Linewidth and Modulation Response

Our analytical treatment of the QD laser linewidth is based on the analysis of the linear response of the dynamical system to small perturbations. These perturbations are naturally present due to spontaneous light emission into the resonator mode. If the statistical variations of the dynamical variables, in our case especially the phase, are known, the optical linewidth can be calculated. There is an elaborate theory on how to determine the statistical variations of the variables in linear stochastic differential equations [20]. If we restrict ourself to the dynamics close to the steady state lasing solution at a fixed injection current, the dynamics of small perturbations from this solution are fully governed by the Jacobian $\mathcal{J}$ of the system, and a simple set of linear ordinary differential equations (ODEs) is left. Defining $\frac{\mathrm{d}\tilde{R}}{\mathrm{d}N} \equiv \frac{\mathrm{d}}{\mathrm{d}N}[R\,(\rho^{eq} - \rho)]$ for brevity and applying some steps of simplification as shown in the appendix A, the Jacobian of our system reads:

$$\mathcal{J} = \begin{pmatrix} -\frac{1}{T_1} - \frac{\mathrm{d}\tilde{R}}{\mathrm{d}N} & R & 0 & 0 \\ \frac{\mathrm{d}\tilde{R}}{\mathrm{d}N} & -R - \frac{1}{T_{sp}} - 4gA^2 & -2(1 + \frac{g(A)}{g_0})\kappa A & 0 \\ 0 & 2gA & -(1 - \frac{g(A)}{g_0})\kappa A & 0 \\ -\delta\Omega & -2g\alpha_0 & -(1 - \frac{g(A)}{g_0})\frac{\kappa}{A}\alpha_0 & 0 \end{pmatrix} \tag{3}$$

The steady state solution of our laser is indicated by $\underline{X}^*$, where $\underline{X}^* = (N^*, \rho^*, A^*, \phi^*)^T$. If evaluated at steady state, (1c) describes the dependence of threshold occupation and gain on the optical field amplitude and we find that $\rho^* = \rho_{\mathrm{th}} = \frac{g(A)+\kappa}{2g(A)}$ is a function of the optical field amplitude A. Applying a perturbation $\underline{P}$ to the system near its fixed point $\underline{X}^*$, we can write down the linear differential equation that describes the equation of motion for the difference vector $\delta\underline{X} = \underline{X} - \underline{X}^*$:

$$\delta\dot{\underline{X}} = \mathcal{J}\delta\underline{X} + \underline{P} \tag{4}$$

An analytical formula for the linewidth can be extracted using the adjoint solution method [39], [40]. Since the linewidth is

mainly given by the optical phase noise [41], [42], our derivation is based on following argumentation. Firstly, the phase response of the system is given by the eigenvector $\underline{e}_\phi$ of the adjoint Jacobian $-J^T$ that is oriented in the direction of the eigensolution of the phase. The eigenvector $\underline{e}_\phi$ projects the total response of the system onto the phase solution. This solution can be identified easily, because (1a)–(1d) do not explicitly depend on ϕ, therefore the phase is an invariant and the eigenvalue λ_ϕ vanishes. This means perturbations can accumulate, leading to a statistical variance σ_ϕ of the phase that increases with time. In statistical terms the phase ϕ performs a random walk while the other variables are described by a damped Ornstein Uhlenbeck process with constant variances that reciprocally depend on the eigenvalue [20]. The linewidth of the optical spectrum is given by the width $\Delta\phi$ of the corresponding normal distribution and is defined as $\Delta\nu = \Delta\phi = \lim_{t\to\infty} \frac{1}{t}\sigma_\phi(t)$. Due to the orthogonality condition of adjoint and nonadjoint solutions, we find that the phase component of the eigenvector $\underline{e}_\phi$ equals unity, specifically $e_{\phi,\phi} = 1$. The phase response $\delta\phi$ is given by the scalar product of $\underline{P}$ and $\underline{e}_\phi$.

In our setup, $\underline{P}$ is a stochastic quantity consisting of Wiener processes $\mathrm{d}W_i$ with noise strengths D_i such that $P_i = D_i \tilde{} \mathrm{d}W_i$. Thus, the average response $\langle\delta\phi\rangle = 0$ vanishes, but the variance $\Delta\phi$ is non-zero and equal to

$$\Delta\phi = \sum_i D_i^2 e_{\phi,i}^2 \tag{5}$$

In the following, we neglect carrier noise in the reservoir and quantum dots and assume spontaneous emission noise $\mathrm{d}\underline{E}|_{sp}$ being the only source of perturbation. $\mathrm{d}\underline{E}|_{sp}$ is modeled using additive complex Gaussian white noise $\xi(t)$ in both the real and imaginary part of the complex electric field plane, such that

$$\mathrm{d}\underline{E}\Big|_{\mathrm{sp}} = D\begin{pmatrix}\xi'\\ \xi''\end{pmatrix}(t) \tag{6}$$

$\xi'(t)$ and $\xi''(t)$ are different realizations of standard Gaussian white noise $\xi(t)$ with mean $\langle\xi(t)\rangle = 0$ and standard deviation $\langle\xi(t)\xi(t')\rangle = \delta(t-t')$. Using Ito's formula [20], $\mathrm{d}\underline{E}|_{sp}$ can be expressed in amplitude and phase noise.

$$\underline{P} = \begin{pmatrix}0\\ 0\\ D\tilde{}\xi'(t)\\ D/A\tilde{}\xi''(t)\end{pmatrix} \tag{7}$$

Applying (5), defining the photon number S as $S \equiv A^2 = |E|^2$, and using $\underline{e}_\phi$ and $\underline{e}_A$ as shown explicitly in the Appendix in (21a), (21b), we extract the phase variance $\Delta\phi$.

$$\Delta\phi = \frac{D^2}{S}\left(1 + \left[\frac{\delta\Omega R}{2g_0(T_1^{-1} + \frac{\mathrm{d}\tilde{R}}{\mathrm{d}N})} + \alpha_0 - \epsilon Q\right]^2\right) \tag{8}$$

with $Q = Q(N) > 0$. More details of the derivation and the explicit expression for Q are given in the Appendix.

In the last step, we use that the phase variance is directly proportional to the linewidth [43], i.e. $\Delta\phi = \Delta\nu$. We identify $\frac{D^2}{S} = \Delta\nu_{\mathrm{ST}}$ as the Schawlow-Townes linewidth limit $\Delta\nu_{\mathrm{ST}}$ and write for our total linewidth $\Delta\nu$:

$$\begin{aligned}\Delta\nu &= \frac{D^2}{S}\left(1 + \left[\frac{\delta\Omega R}{2g_0(T_1^{-1} + \frac{\mathrm{d}}{\mathrm{d}N}[R(\rho^{eq} - \rho)])} + \alpha_0 - \epsilon Q\right]^2\right)\\ &\equiv \Delta\nu_{\mathrm{ST}}(1+\alpha^2)\end{aligned} \tag{9}$$

In (9) three contributions to the linewidth enhancement factor α can be seen. Using the definition

$$\alpha_{\mathrm{dyn}} = \frac{\delta\Omega R}{2g_0(T_1^{-1} + \frac{\mathrm{d}}{\mathrm{d}N}[R(\rho^{eq} - \rho)])} \tag{10}$$

we obtain:

$$\alpha(N) = \alpha_0 + \alpha_{\mathrm{dyn}}(N) - \epsilon Q(N) \tag{11}$$

The first term in (11) is due to the commonly known linear amplitude phase coupling and adequately describes the linewidth of a quantum well laser [25] (case $\delta\Omega = 0$). The second term describes our nonlinear dynamical correction $\alpha_{\mathrm{dyn}}(N)$ and is directly connected to the frequency shifts $\omega_{\mathrm{I,ES}} = -\delta\Omega N$ that arise dynamically from the scattering of carriers in the QD and reservoir states. The clear dependence of $\alpha_{\mathrm{dyn}}(N)$ on the scattering rates $R(N)$, and $\rho^{eq}(N)$ underlines the nonlinear nature of the QD laser linewidth. The last term is an additional correction that arises due to gain compression. Note that the gain compression also changes α_{dyn} as it changes the carrier density itself. In contrast to the rate equation model in [10] our formula is not limited to empty QDs or a linear dependence of the scattering rate on the injection current. Instead, (9) holds for every dependence $R(N)$, as long as the scattering rate is mainly a function of the reservoir charge carriers. The specific case of the QD laser that is investigated in the experiments will be discussed in the next section.

The characterization of a QD laser is often also done by measuring modulation response curves, i.e. transfer functions. The modulation response transfer function is calculated (similar to [43] for a 2 variable system) in a small signal analysis calculus and defined as $H(\omega) := |\frac{\delta S(\omega)}{\delta S(0)}|^2$.

Here, $\delta S(\omega)$ describes the response of the electric field intensity $S = A^2 = |E|^2$ to a small modulation of the injection current $J = J_{\mathrm{DC}} + \delta J\exp(-i\omega t)$. Following the same approach used for the linewidth calculations and using the same abbreviation $\frac{\mathrm{d}\tilde{R}}{\mathrm{d}N} \equiv \frac{\mathrm{d}}{\mathrm{d}N}[R(\rho^{eq} - \rho)]$, we find:

$$\begin{aligned}\frac{\delta S(\omega)}{\delta J(\omega)} = &\frac{4gS\frac{\mathrm{d}\tilde{R}}{\mathrm{d}N}}{-i\omega + T_1^{-1} + \frac{\mathrm{d}\tilde{R}}{\mathrm{d}N}} \times\\ &\frac{1}{(-\omega^2 + \frac{i\omega R\frac{\mathrm{d}\tilde{R}}{\mathrm{d}N}}{-i\omega + T_1^{-1} + \frac{\mathrm{d}\tilde{R}}{\mathrm{d}N}} - i\omega(R + T_{\mathrm{sp}}^{-1} + 2gS) + 4g\kappa S)}\end{aligned} \tag{12}$$

Similar to the linewidth, also the modulation response strongly depends on the scattering rates and their derivatives with respect to the carrier density. The additional dependency of the scattering rate on the reservoir carrier density leads to a higher value of $\frac{\mathrm{d}\tilde{R}}{\mathrm{d}N}$, which in turn improves the modulation response at higher

frequencies. In contrast, models that assume constant scattering rates [18], [19] would therefore predict a lower modulation bandwidth.

IV. Comparison Between Experiment and Theory

The optical linewidth measurements have been performed on a distributed feedback laser with InAs quantum dots grown on InP substrate [45]. The InAs/InP QD DFB laser used in this study was grown by chemical beam epitaxy (CBE) on a (100) oriented n-type InP substrate. The undoped active region of the laser consisted of five stacked layers of InAs QDs with 30 nm $In_{0.816}Ga_{0.184}As_{0.392}P_{0.608}$ (1.15Q) barriers. The QDs were tuned to operate in the desirable operation wavelength range by using a QD double cap growth procedure and a GaP sublayer [46]. Growing the dots on a thin GaP layer allows a high dot density to be obtained and improved layer uniformity when stacking multiple layers of dots, providing maximum gain. This active layer was embedded in a 350 nm thick 1.15Q waveguiding core, providing both carrier and optical confinement. An average dot density of approximately 4×10^{10} cm^{-2} per layer was obtained according to atomic force microscopy (AFM) measurements on uncapped stacked dot samples. Following the growth of the QD active core the wafer was removed to pattern the grating region. This was performed using a HeCd laser to holographically expose the uniform grating pattern across the whole wafer, followed by wet chemical etching. Following the patterning of the grating the p-type InP cladding and InGaAs contact layers were regrown using metal-organic chemical vapour deposition (MOCVD). Single lateral mode ridge waveguide lasers were fabricated with a stripe width of 3 μm and cavity length of 1 mm, and the facets coated to provide 2% and 62% reflectivity. The threshold current is 39 mA at 20 °C, with an external efficiency of 14%. The experimental setup is sketched in Fig. 2. The laser is biased with a low noise current source. The output light is coupled into the interferometer by using an AR coated lens-ended fiber. In order to avoid any external feedback into the DFB cavity, two cascaded isolators are applied for an isolation greater than 60 dB. Once the laser emission is launched into the fiber interferometer, half of the signal is sent to a 100 MHz frequency-shifted acousto-optic modulator (AOM) while the other half propagates through a 25 km fiber coil. The polarization controller is used to match the polarizations in the two arms. At the output of the interferometer, the optical signals from the two arms are mixed and the resulting beat note centered at the AOM frequency is measured with an electrical spectrum analyzer and a slow photo detector. Fig. 3 shows a typical spectrum obtained from our setup. The linewidth data is extracted using a Voigt fit [44].

As discussed in Section III our model is able to capture both the carrier dynamics which is accessible via injection current modulation as well as the dynamics of the electric field to perturbations measured as the laser linewidth. Thus we now compare those calculations with experimental data. To obtain a quantitative agreement some parameters had to be fitted to the experimental data. Losses, gain and the effective scattering rate parameter where chosen to fit the light vs injected pump current characteristics (LI-curve) of our numerical integration at first. Secondly, we extract the T_1 time and $\frac{\mathrm{d}\bar{R}}{\mathrm{d}N}$ using the modulation response in (13a). The ratio of g and κ were iteratively adjusted to achieve agreement with the LI-curve. In a third step, the data from our linewidth measurements, see Fig. 6, yields value for the index shift $\delta\Omega$, the linear amplitude phase coupling coefficient α_0 and the noise strength D.

TABLE I.
Parameters of the QD Laser Devices

Parameter	(Description)	Value [unit]
R_{th}	(scattering rate at threshold)	1200 [ns^{-1}]
$\frac{\mathrm{d}R}{\mathrm{d}N}$	(differential eff. sc. rate)	550 [ns^{-1}]
$\frac{\mathrm{d}R^{\mathrm{in}}}{\mathrm{d}N}$	(differential in-sc. rate)	550×0.675 [ns^{-1}]
T_1	(reservoir carrier lifetime)	0.25 [ns]
T_{sp}	(spontaneous emission lifetime)	4 [ns]
g_0	(gain coefficient at threshold)	234 [ns^{-1}]
κ	(electric field losses)	58.6 [ns^{-1}]
ε	(gain compression coefficient)	0.28
$\delta\Omega$	(reservoir carrier frequency shift)	18 [GHz]
α_0	(linear amp.-phase coupling)	0
D^2	(spont. emission noise power)	5.85 [kHz]
J_{th}	(pump current at threshold)	48 [mA]

Note: All parameters are obtained from the regression of our model to the experimental measurements.

The parameters given in Table I define one single parameter set that was applied to all simulations and calculations.

In Fig. 4(a) and (b) the experimental data for the modulation response and the LI characteristics of the QD laser are shown. Superimposed are the modeling results after applying the fitting procedure. The transfer function in Fig. 4(a) shows a resonance peak, which is close to the relaxation oscillation frequency. Its maximum shifts towards higher frequencies with increasing injection current (see lines in Fig. 4(a) from bottom to top), consequently increasing the 3dB-cutoff frequency of the QD laser. This is due to the increasing scattering rates and photon densities which lead to a higher resonance frequency and improve the modulation capabilities of the QD laser [17], [19], [47]. Small deviations between experiment and theory for intermediate pump currents arise from the minimalistic model approach. A more complex model, including for instance excited or inactive QD states or a sepereate treatment of electrons and holes would improve the agreement to the experimental data, but also increase the complexity of the calculations drastically. In favor of simplicity, the minimalistic approach is the means of choice. The power dependence in Fig. 4(b) shows a significant saturation at elevated currents as can be seen from the down bending of the output power $S(J)$. This effect is captured by the gain compression in our model. Choosing a value of $\varepsilon = 0.28$ leads to a very good agreement, as can be seen by comparing the dashed and solid line for theory and experiment, respectively, in Fig 4(b).

However, the seemingly low moderate saturation of the LI-curve hides the strong effect of the gain compression ϵ on the carrier distribution within the laser device. This can better be seen by looking at the steady states of the charge carriers N and scattering rates R which are accessible via numerically solving the differential equation system (1). The simulated steady state

results of $R(J), N(J), \rho^{eq}(J)$ and $g(J)$ are displayed in Fig. 5 as a function of the pump current. To highlight the effect of the gain compression also the results for the case $\epsilon = 0$ are shown with dashed curves. It can be seen that the compression of the gain increases the steady state density of the carriers in the reservoir (green line in Fig. 5(a)). The reason is the nonlinear gain which nonlinearly decreases with the photon number (2) and thus with the injection current (black curve in Fig. 5(b)). This decrease is balanced by a stronger increase of the carrier densities if compared to the case without gain compression. As a consequence the carrier dependent scattering rates and the reservoir carrier densities itself show an approximately quadratic increase with the injection current in Fig. 5(a). As the equilibrium occupation of the QD levels ρ^{eq} is given by a detailed balance between in- and out scattering rates, it is also a function of the carrier densities and is thus nonlinearly increasing with the pump current (green line in Fig. 5(b)) .

To take the gain compression induced nonlinearities correctly into account, we feed the analytical formula (9) with the numerically obtained values shown in Fig. 5, in particular $R(J)$ and $S(J)$ (note that $\frac{\mathrm{d}\tilde{R}}{\mathrm{d}N} = const.$) and calculate the QD laser linewidth. Due to the nonlinear dependencies, the semi-analytically calculated curve for the linewidth does not scale inversely proportional to the injection currents, and instead shows a rebroadening of the linewidth at elevated currents. This can be seen in Fig. 6, where the linewidth is plotted as a function of the injected pump current. The plot shows both experimental (symbols) and semi-analytical data (solid line) which show a very good agreement. Since we have the analytic expression for the linewidth, our modeling is not only able to reproduce the experimental findings, it is also able to explain the reasoning for the rebroadening.

For low injection currents (below $1.5J_{\mathrm{th}}$), the system is dominated by spontaneous emission noise and obeys the limit $\Delta\nu \xrightarrow[J\to J_{\mathrm{th}}]{} \infty$. At approx. $J \approx 75\,\mathrm{mA} \approx 1.5J_{\mathrm{th}}$, we find a minimal laser linewidth of less than 200 kHz. For higher injection currents, the laser line rebroadens, such that its value is doubled at $J \approx 3J_{\mathrm{th}} \approx 150$ mA (Fig. 6). This behavior is quite different from conventional laser diodes, which typically show a saturation of the linewidth at higher pump current. Equation (9) allows us to identify the driving mechanism for this effect to be the carrier dependent scattering rates $R(N)$ which increase with the slope $\frac{\mathrm{d}\tilde{R}}{\mathrm{d}N}$ and consequently broaden the linewidth after its initial decrease.

The effect of the gain compression ϵ on the linewidth is more intricate. We already mentioned that there are two competing mechanisms identified in (9), i.e. the direct dependence on ϵ that reduces the linewidth via the correction term ϵQ and the indirect effect of ϵ on the carrier density N that leads to an increasing linewidth. For the latter the saturation of the gain implies a nonlinear increase of the carriers at high intensities and thus a nonlinear increase of the scattering rates. However, for realistic parameters the gain compression coefficient in QD lasers leads to a net broadening of the linewidth.

To make the effect of ϵ more visible, we varied the gain compression from $\varepsilon = 0$ to 0.5 in Fig. 7 and calculated the value of the different contributions to the linewidth. In Fig. 7(a) we plot

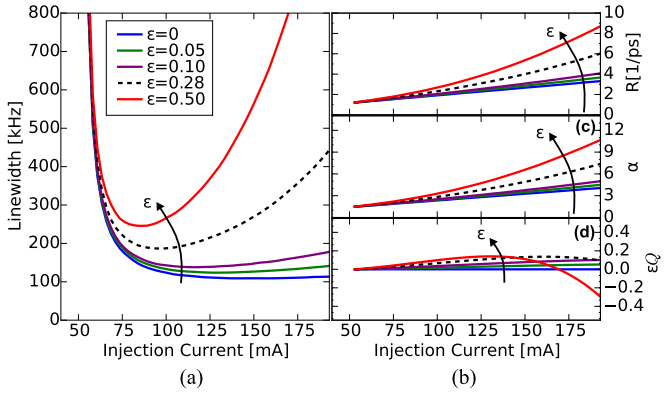

Fig. 7. Contributions to the linewidth rebroadening: (a) linewidth as a function of the pump current as given in (9), different colors correspond to different ε, (b) –(d) show the contributions $R(J)$, $\alpha_{dyn}(J)$, and $\epsilon Q(J)$ to the linewidth, respectively. Dashed curves show the discussed case for our QD laser parameterset, with $\varepsilon = 0.28$.

the total linewidth as a function of the injection current (different colors indicate different ϵ values), while the different contributions to the linewidth are shown in Fig. 7(b)–(d) (namely R, α_{dyn} and ϵQ). For $\varepsilon = 0$ (blue lines in Fig. 7) the linewidth shows only a slight increase at higher currents, suggesting that gain saturation is the main cause for the rebroadening of the laser line. Nevertheless, having a closer look to the different numerically computed contributions to the linewidth, a different picture develops. At first it can be seen that the effective scattering rates R increases much stronger with J as soon as ϵ is nonzero. Also the semi-analytically calculated α_{dyn}-factor in Fig. 7(c) is enhanced by the gain compression ε due to its nonlinear dependence on the charge carrier densities N (for nonzero ϵ, N increases with pump current to compensate for the reduced gain). Instead the correction term ϵQ from (9) that is plotted in Fig. 7(d) has a much smaller contribution (see ticks in the y-axis) and changes only slightly. In the given example of maximal gain compression $\epsilon_{\max} = 0.5$ we find a maximum correction of $\epsilon Q = -0.35$ which is less than 5% of the corresponding α (approximately 9). Therefore we can conclude that the rebroadening of the laser linewidth can be predominantly attributed to the dependence of the scattering rates R on N and thereby also on J. For constant scattering rates $R(J) = const$ even strong gain compression could not induce a rebroadening.

V. Analytics in the Limit of No Gain Compression

In this last section we will derive an analytic equation that allows to directly extract values for the current dependent α-factor and scattering rates from the measurements discussed so far, i.e. from LI-curve, modulation response and linewidth measurements. Compared to pump-probe setups or other more involved techniques that are usually used to gain information about the internal scattering processes, these measurements can be done easily with standard techniques.

To be able to do that we need to assume a QD laser that exhibit comparably lower gain compression. In this case (9) can be treated in a fully analytical manner. Assuming $\varepsilon = 0$, the reservoir carrier density N increases linearly with the pump current J and the microscopically motivated scattering rates

$e_{A,\phi}$

$$= \frac{\alpha_0 T_{\rm sp}\Big(4\left(A^2+1\right)g^2(\frac{\mathrm{d}\tilde{R}}{\mathrm{d}N}T_1+1)+g\Big(R-4\left(A^2-1\right)g_0(\frac{\mathrm{d}\tilde{R}}{\mathrm{d}N}T_1+1)\Big)-g_0R\Big)+\alpha_0(\frac{\mathrm{d}\tilde{R}}{\mathrm{d}N}T_1+1)(g-g_0)-2\delta\Omega RT_1T_{\rm sp}(g+g_0)}{4(A-1)Ag^2T_{\rm sp}(\frac{\mathrm{d}\tilde{R}}{\mathrm{d}N}T_1+1)+g(T_{\rm sp}(R-4A(A+1)g_0(\frac{\mathrm{d}\tilde{R}}{\mathrm{d}N}T_1+1))+\frac{\mathrm{d}\tilde{R}}{\mathrm{d}N}T_1+1)-g_0(\frac{\mathrm{d}\tilde{R}}{\mathrm{d}N}T_1+RT_{\rm sp}+1)} \tag{19a}$$

$$e_{\phi,\phi}=1 \tag{19b}$$

$R(N)$ are in a good approximation also linearly proportional to the pump current (in contrast to the nonlinear scattering rates used in our model and shown in Fig. 5(a)). We can thus write:

$$R(J)=R_{\rm th}+\left.\frac{\mathrm{d}R}{\mathrm{d}J}\right|_{\rm th}(J-J_{\rm th}) \tag{13a}$$

$$R^{\rm in}(J)=R^{\rm in}_{\rm th}+\left.\frac{\mathrm{d}R^{\rm in}}{\mathrm{d}J}\right|_{\rm th}(J-J_{\rm th}) \tag{13b}$$

This restriction to linear LI-curves also covers the modeling of R as in [19] ($\frac{\mathrm{d}R}{\mathrm{d}N}=0$, $\frac{\mathrm{d}\rho^{eq}}{\mathrm{d}N}$ =const.) and [10] ($\frac{\mathrm{d}R}{\mathrm{d}N}=\frac{\mathrm{d}R^{\rm in}}{\mathrm{d}N}$).

This approximation also allows an easy access to information about the scattering rates. From (1a), the analytical equation for the LI-curve derived from (1a)–(1c) at steady state reads:

$$S(J)=\frac{1}{2\kappa}\left[R^{\rm in}(J)-\rho_{\rm th}\left(R(J)+\frac{1}{T_{sp}}\right)\right] \tag{14}$$

This equation can be used to derive a simplified version of (9). We find that α in dependence of J yields (Please see Appendix for the derivation):

$$\alpha(J)=\alpha_0+\frac{\delta\Omega T_1}{2g}\left(1-\frac{\mathrm{d}(2\kappa S)}{\mathrm{d}J}\right)R(J)\propto J \tag{15}$$

Interestingly, we see that $\frac{\mathrm{d}(2\kappa S)}{\mathrm{d}J}=\frac{e_0}{\hbar\omega}\frac{\mathrm{d}P}{\mathrm{d}I}$, where $\frac{\mathrm{d}P}{\mathrm{d}I}$ is the slope efficiency of the laser, e.g. the ratio of the differential output power ∂P divided by differential pump current increment ∂I. The slope efficiency can be obtained by measurements of the LI-curve (including detector efficiencies, fiber, coupling and other losses). As shown in Fig. 4, the factors T_1, g and $R(J)$ can be obtained by fitting the modulation response of the QD laser. As $\frac{\mathrm{d}\tilde{R}}{\mathrm{d}N}$ is already given by the LI-curve, the peak of the maximum in (13a) is predominantly given by T_1, while its position (or similarly the position of the 3dB-cutoff frequency $\omega_{\rm 3dB}$ depends on $\frac{\mathrm{d}\tilde{R}}{\mathrm{d}J}$, allowing these two quantities to be fitted with good accuracy.

In the last step, we take into account, that $(1+\alpha^2)$ is a second order polynomial of J. The Schawlow-Townes linewidth limit is solely given by the output power P and device constants [25], [31], [42], [43]. Therefore we can fit

$$\frac{\Delta\nu}{\Delta\nu_{ST}}=(1+\alpha(J)^2) \tag{16}$$

using (15). This allows us to determine the dynamical α-factor given by (10) (for $\epsilon=0$):

$$\alpha_{\rm dyn}=\delta\Omega\frac{T1}{2g}(1-\frac{e_0}{\hbar\omega}\frac{\mathrm{d}P}{\mathrm{d}I})R(J) \tag{17}$$

As $R(J)$ is already quantified by the LI-curve (14) and the modulation response from (13a), above (17) yields the remaining free parameter $\delta\Omega$, such that the QD laser is fully described within the minimal rate equation model. As shown, all parameters are extracted from the presented, simple measurements.

VI. Conclusion

Using a minimal quantum dot laser model, we derived semi-analytic expressions that reproduce LI curves modulation response data, as well as the laser linewidth. We intuitively explain a linewidth rebroadening process in QD lasers due to a dynamically growing linewidth enhancement factor α that is caused by the increasing scattering rates between the QD and the reservoir states. Additionally, we showed that the combination of three relatively simple experiments, namely modulation response, linewidth and LI measurements is sufficient to extract most important parameters, including effective scattering rates in the QD device. Our derived analytical results help characterize the laser devices, including the internal carrier time scales without the need for expensive, high- or real-time-resolution measurements.

A. Appendix

A. Additional Information to the Linewidth Formula

We derive the linewidth formula, based on the adjoint method approach, given in Section II. Based on (1a)–(1d), we find the full Jacobian at steady state:

$$\mathcal{J}=\begin{pmatrix} -\frac{1}{T_1}-\frac{\mathrm{d}\tilde{R}}{\mathrm{d}N} & R & R0 & 0 \\ \frac{\mathrm{d}\tilde{R}}{\mathrm{d}N} & -R-\frac{1}{T_{sp}}-4gA^2 & -4\kappa A-2\frac{\partial g}{\partial A}(2\rho-1)A^2 & 0 \\ 0 & 2gA & \text{“0”}+\frac{\partial g}{\partial A}(2\rho-1)A^2 & 0 \\ -\delta\Omega & -2g\alpha_0 & \frac{\partial g}{\partial A}(2\rho-1)\alpha_0 & 0 \end{pmatrix} \tag{18}$$

In (18), all contributions of $\frac{\partial g}{\partial A}$ emerge from the gain compression term. Therefore, $\frac{\partial g}{\partial A}=-\epsilon\frac{g_0A}{(1+\epsilon A^2)^2}=\frac{-\varepsilon A}{1+\varepsilon A^2}\,g(A)\,A$. Using ρ at steady state $\rho^*=\frac{g+\kappa}{2g}$, we find that $2\frac{\partial g}{\partial A}(2\rho-1)A^2=2(1-\frac{g(A)}{g_0})\kappa A$. Therefore, the Jacobian $\mathcal{J}$ can be simplified, as written in (3).

The eigenvectors used in (5) are obtained by calculating the eigenvectors and eigenvalues of $\mathcal{J}$, (3), via Mathematica10.1, in full precision they read as shown in (19a), (19b), as shown at the top of the page.

$$Q = -\frac{4A^4\alpha_0\frac{\mathrm{d}\tilde{R}}{\mathrm{d}N}g_0T_1T_{\mathrm{sp}}+4A^4\alpha_0g_0T_{\mathrm{sp}}-4A^2\alpha_0\frac{\mathrm{d}\tilde{R}}{\mathrm{d}N}g_0T_1T_{\mathrm{sp}}+A^2\alpha_0\frac{\mathrm{d}\tilde{R}}{\mathrm{d}N}T_1-4A^2\alpha_0g_0T_{\mathrm{sp}}+A^2\alpha_0RT_{\mathrm{sp}}+A^2\alpha_0+6A^2\delta\Omega RT_1T_{\mathrm{sp}}}{8g_0T_{\mathrm{sp}}(\frac{\mathrm{d}\tilde{R}}{\mathrm{d}N}T_1+1)} + \frac{\left(T_{\mathrm{sp}}\left(4\left(A^3+A^2\right)g_0(\frac{\mathrm{d}\tilde{R}}{\mathrm{d}N}T_1+1)+AR\right)+A\frac{\mathrm{d}\tilde{R}}{\mathrm{d}N}T_1+A\right)(-8\alpha_0\frac{\mathrm{d}\tilde{R}}{\mathrm{d}N}g_0T_1T_{\mathrm{sp}}-8\alpha_0g_0T_{\mathrm{sp}}+4\delta\Omega RT_1T_{\mathrm{sp}})}{64{g_0}^2{T_{\mathrm{sp}}}^2(\frac{\mathrm{d}\tilde{R}}{\mathrm{d}N}T_1+1)^2} \tag{20}$$

For brevity, we also show the electric field amplitude and phase component of the eigenvectors $e_{A,\phi}$ and $e_{\phi,\phi}$ in a first order Taylor approximation in ε around $\varepsilon = 0$, as used in (9). To make the eigenvalues more readable we define a correction term Q that is given by (20), shown at the top of the page. Using this abbreviation for Q the eigenvalues read:

$$e_{A,\phi} = \frac{1}{A}\left(\frac{\delta\Omega R}{2g_0(T_1^{-1}+\frac{\mathrm{d}\tilde{R}}{\mathrm{d}N})}+\alpha_0-\epsilon Q\right) \tag{21a}$$

$$e_{\phi,\phi} = 1 \tag{21b}$$

Our simulations show that Q is comparatively small, see Fig. 7(d). As defined in (21), εQ describes the reduction of $\alpha = \alpha_0 + \alpha_{\mathrm{dyn}} - \varepsilon Q$. Our results give a correction to α of less than 5%.

B. Derivation of the Simplified Equation for α

For the derivation of the simplified (15) of α, we use the assumption for $R(J)$ in (13) to calculate the LI-curve. From $\dot{\rho}$ and $\rho_{\mathrm{th}} = \frac{g+\kappa}{2g} = \mathrm{const.}$, (1b) reads $\dot{\rho} = 0 = R(\rho^{eq} - \rho_{\mathrm{th}}) - \frac{\rho_{\mathrm{th}}}{T_{\mathrm{sp}}} - 2\kappa S$, and therefore

$$S = \frac{1}{2\kappa}(\underbrace{R(\rho^{eq}}_{R^{\mathrm{in}}} - \rho_{\mathrm{th}}) - \frac{\rho_{\mathrm{th}}}{T_{\mathrm{sp}}}) \tag{22a}$$

$$= \frac{1}{2\kappa}(R^{\mathrm{in}} - \rho_{\mathrm{th}}(R + T_{\mathrm{sp}}^{-1})) \tag{22b}$$

Since ρ_{th} is constant, derivation of S after J gives

$$\frac{\mathrm{d}(2\kappa S)}{\mathrm{d}J} = \frac{\mathrm{d}R(\rho^{eq}-\rho_{\mathrm{th}})}{\mathrm{d}J} = \frac{\mathrm{d}\tilde{R}}{\mathrm{d}J} \tag{23}$$

To calculate $\alpha(J)$, the factor $\frac{\mathrm{d}\tilde{R}}{\mathrm{d}J}$ must be converted into δR. We use the chain rule $\frac{\mathrm{d}\tilde{R}}{\mathrm{d}J} = \frac{\mathrm{d}\tilde{R}}{\mathrm{d}N}\frac{\mathrm{d}N}{\mathrm{d}J}$. The latter term $\frac{\mathrm{d}N}{\mathrm{d}J}$ is given by the carrier conservation, that reads $\dot{N} + \dot{\rho} + \dot{S} = 0$.

$$J = \frac{N}{T_1} + \frac{\rho_{\mathrm{th}}}{T_{\mathrm{sp}}} + 2\kappa S \tag{24a}$$

$$\Rightarrow \frac{\mathrm{d}N}{\mathrm{d}J} = T_1\left(1 - \frac{\mathrm{d}(2\kappa S)}{\mathrm{d}J}\right) \tag{24b}$$

Thus,

$$\begin{aligned}\alpha &= \alpha_0 + \frac{\delta\Omega}{2g}\frac{1}{T_1^{-1}+\frac{\mathrm{d}\tilde{R}}{\mathrm{d}N}}R(J)\\ &= \alpha_0 + \frac{\delta\Omega}{2g}\frac{1}{T_1^{-1}+\frac{\mathrm{d}R}{\mathrm{d}J}/\frac{\mathrm{d}N}{\mathrm{d}J}}R(J)\\ &= \alpha_0 + \frac{\delta\Omega}{2g}\frac{1}{T_1^{-1}+\frac{\frac{\mathrm{d}(2\kappa S)}{\mathrm{d}J}}{T_1(1-\frac{\mathrm{d}(2\kappa S)}{\mathrm{d}J})}}R(J)\end{aligned} \tag{25}$$

which is identical to (15).

REFERENCES

[1] J. J. Coleman, J. D. Young, and A. Garg, "Semiconductor quantum dot lasers: A tutorial," *J. Lightw. Technol.*, vol. 29, no. 4, pp. 499–510, Feb. 2011.

[2] W. W. Chow and F. Jahnke, "On the physics of semiconductor quantum dots for applications in lasers and quantum optics," *Prog. Quantum Electron.*, vol. 37, pp. 109–184, 2013.

[3] D. Bimberg, *Semiconductor Nanostructures*. Berlin, Germany: Springer, 2008.

[4] T. Erneux and P. Glorieux, *Laser Dynamics*. Cambridge, U.K.: Cambridge Univ. Press, 2010.

[5] M. Osinski and J. Buus, "Linewidth broadening factor in semiconductor lasers—An overview," *IEEE J. Quantum Electron.*, vol. QE-23, no. 1, pp. 9–29, Jan. 1987.

[6] W. W. Chow and S. W. Koch, *Semiconductor-Laser Fundamentals*. Berlin, Germany: Springer, 1999.

[7] C. H. Henry, "Theory of the linewidth of semiconductor lasers," *IEEE J. Quantum Electron.*, vol. QE-18, no. 2, pp. 259–264, Feb. 1982.

[8] B. Lingnau, K. Lüdge, W. W. Chow, and E. Schöll, "Failure of the α-factor in describing dynamical instabilities and chaos in quantum-dot lasers," *Phys. Rev. E*, vol. 86, no. 6, 2012, Art. no. 065201(R).

[9] B. Lingnau, W. W. Chow, and K. Lüdge, "Amplitude-phase coupling and chirp in quantum-dot lasers: influence of charge carrier scattering dynamics," *Opt. Express*, vol. 22, no. 5, pp. 4867–4879, 2014.

[10] S. Melnik, G. Huyet, and A. V. Uskov, "The linewidth enhancement factor α of quantum dot semiconductor lasers," *Opt. Express*, vol. 14, no. 7, pp. 2950–2955, 2006.

[11] M. Gioannini, A. Sevega, and I. Montrosset, "Simulations of differential gain and linewidth enhancement factor of quantum dot semiconductor lasers," *Opt. Quantum Electron.*, vol. 38, pp. 381–394, 2006.

[12] M. Gioannini and I. Montrosset, "Numerical analysis of the frequency chirp in quantum-dot semiconductor lasers," *IEEE J. Quantum Electron.*, vol. 43, no. 10, pp. 941–949, Oct. 2007.

[13] F. Grillot, B. Dagens, J. G. Provost, H. Su, and L. F. Lester, "Gain compression and above-threshold linewidth enhancement factor in 1.3 μm InAs/GaAs quantum-dot lasers," *IEEE J. Quantum Electron.*, vol. 44, no. 10, pp. 946–951, Oct. 2008.

[14] C. Wang, B. Lingnau, K. Lüdge, J. Even, and F. Grillot, "Enhanced dynamic performance of quantum dot semiconductor lasers operating on the excited state," *IEEE J. Quantum Electron.*, vol. 50, no. 9, pp. 723–731, Sep. 2014.

[15] C. Wang, J. P. Zhuang, F. Grillot, and S. C. Chan, "Contribution of off-resonant states to the phase noise of quantum dot lasers," *Opt. Express*, vol. 24, pp. 29872–29881, Dec. 2016.

[16] G. S. Sokolovskii *et al.*, "Nonvanishing turn-on delay in quantum dot lasers," *Appl. Phys. Lett.*, vol. 100, no. 8, 2012, Art. no. 081109.
[17] K. Lüdge, E. Schöll, E. A. Viktorov, and T. Erneux, "Analytic approach to modulation properties of quantum dot lasers," *J. Appl. Phys.*, vol. 109, no. 9, 2011, Art. no. 103112.
[18] C. Wang, F. Grillot, and J. Even, "Impacts of wetting layer and excited state on the modulation response of quantum-dot lasers," *IEEE J. Quantum Electron.*, vol. 48, no. 9, pp. 1144–1150, Sep. 2012.
[19] B. Lingnau and K. Lüdge, "Analytic characterization of the dynamic regimes of quantum-dot lasers," *Photonics*, vol. 2, no. 2, pp. 402–413, 2015.
[20] C. W. Gardiner, *Handbook of Stochastic Methods for Physics, Chemistry and the Natural Sciences*. Berlin, Germany: Springer, 2002.
[21] H. Haken, *Laser Light Dynamics*, vol. I, 1st ed. Amsterdam, The Netherlands: North Holland, 1986.
[22] B. Lingnau, W. W. Chow, E. Schöll, and K. Lüdge, "Feedback and injection locking instabilities in quantum-dot lasers: A microscopically based bifurcation analysis," *New J. Phys.*, vol. 15, 2013, Art. no. 093031.
[23] M. Lorke, F. Jahnke, and W. W. Chow, "Excitation dependences of gain and carrier-induced refractive index change in quantum-dot lasers," *Appl. Phys. Lett.*, vol. 90, 2007, Art. no. 051112.
[24] W. W. Chow and S. W. Koch, "Theory of semiconductor quantum-dot laser dynamics," *IEEE J. Quantum Electron.*, vol. 41, no. 4, pp. 495–505, Apr. 2005.
[25] A. Yariv, *Optical Electronics in Modern Communications*. London, U.K.: Oxford Univ. Press, 1997.
[26] J. Ohtsubo, *Semiconductor Lasers: Stability, Instability and Chaos*. Berlin, Germany: Springer, 2005.
[27] K. Lüdge and E. Schöll, "Quantum-dot lasers-desynchronized nonlinear dynamics of electrons and holes," *IEEE J. Quantum Electron.*, vol. 45, no. 11, pp. 1396–1403, Oct. 2009.
[28] T. R. Nielsen, P. Gartner, and F. Jahnke, "Many-body theory of carrier capture and relaxation in semiconductor quantum-dot lasers," *Phys. Rev. B*, vol. 69, 2004, Art. no. 235314.
[29] N. Majer *et al.*, "Impact of carrier-carrier scattering and carrier heating on pulse train dynamics of quantum dot semiconductor optical amplifiers," *Appl. Phys. Lett.*, vol. 99, 2011, Art. no. 131102.
[30] A. Wilms, D. Breddermann, and P. Mathe, "Theory of direct capture from two- and three-dimensional reservoirs to quantum dot states," *Phys. Status Solidi C*, vol. 9, no. 5, pp. 1278–1280, 2012.
[31] Z. Toffano, A. Destrez, C. Birocheau, and L. Hassine, "New linewidth enhancement determination method in semiconductor lasers based on spectrum analysis above and below threshold," *Electron. Lett.*, vol. 28, pp. 9–11, Jan. 1992.
[32] T. Fordell and A. M. Lindberg, "Experiments on the linewidth-enhancement factor of a vertical-cavity surface-emitting laser," *IEEE J. Quantum Electron.*, vol. 43, no. 1, pp. 6–15, Jan. 2007.
[33] M. Sciamanna, P. Mégret, and M. Blondel, "Hopf bifurcation cascade in small-α laser diodes subject to optical feedback," *Phys. Rev. E*, vol. 69, Apr. 2004, Art. no. 046209.
[34] C. Masoller and M. S. Torre, "Influence of optical feedback on the polarization switching of vertical-cavity surface-emitting lasers," *IEEE J. Quantum Electron.*, vol. 41, no. 4, pp. 483–489, Apr. 2005.
[35] G. Huyet *et al.*, "Quantum dot semiconductor lasers with optical feedback," *Phys. Status Solidi B*, vol. 201, no. 2, pp. 345–352, 2004.
[36] M. Gioannini, A. Sevega, and I. Montrosset, "Simulations of differential gain and linewidth enhancement factor of quantum dot semiconductor lasers," *Opt. Quantum Electron.*, vol. 38, no. 4, pp. 381–394, 2006.
[37] A. V. Uskov *et al.*, "Carrier-induced refractive index in quantum dot structures due to transitions from discrete quantum dot levels to continuum states," *Appl. Phys. Lett.*, vol. 84, no. 2, pp. 272–274, 2004.
[38] S. P. Hegarty, B. Corbett, J. G. McInerney, and G. Huyet, "Free-carrier effect on index change in $1.3/mum$ quantum-dot lasers," *Electron. Lett.*, vol. 41, no. 7, pp. 416–418, 2005.
[39] L. C. Jaurigue *et al.*, "Timing jitter of passively mode-locked semiconductor lasers subject to optical feedback; a semi-analytic approach," *Phys. Rev. A*, vol. 92, no. 5, 2015, Art. no. 053807.
[40] A. S. Pimenov *et al.*, "The effect of dynamical instability on timing jitter in passively mode-locked quantum-dot lasers," *Opt. Lett.*, vol. 39, no. 24, pp. 6815–6818, 2014.
[41] C. H. Henry, "Theory of the phase noise and power spectrum of a single mode injection laser," *IEEE J. Quantum Electron.*, vol. QE-19, no. 9, pp. 1391–1397, Sep. 1983.
[42] H. Gerhardt, H. Welling, and A. Güttner, "Measurements of the laser linewidth due to quantum phase and quantum amplitude noise above and below threshold. i," *Zeitschrift für Physik*, vol. 253, no. 2, pp. 113–126, 1972.
[43] L. A. Coldren, S. W. Corzine, and M. Mashanovitch, *Diode Lasers and Photonic Integrated Circuits* (Wiley series in Microwave and Optical Enginieering), 2nd ed. New York, NY, USA: Wiley, 2012.
[44] T. Ida, M. Ando, and H. Toraya, "Extended pseudo-Voigt function for approximating the Voigt profile," *J. Appl. Crystallography*, vol. 33, pp. 1311–1316, Dec. 2000.
[45] Z. G. Lu *et al.*, "High-performance 1.52 μm InAs/InP quantum dot distributed feedback laser," *Electron. Lett.*, vol. 47, pp. 818–819, Jul. 2011.
[46] P. J. Poole, K. Kaminska, P. Barrios, Z. Lu, and J. Liu, "Growth of InAs/InP-based quantum dots for 1.55 μm laser applications," *J. Crystal Growth*, vol. 311, no. 6, pp. 1482–1486, 2009.
[47] L. V. Asryan, Y. Wu, and R. A. Suris, "Carrier capture delay and modulation bandwidth in an edge-emitting quantum dot laser," *Appl. Phys. Lett.*, vol. 98, 2011, Art. no. 131108.

Christoph Redlich received the B.Sc. degree in physics from the Institute of Optics and Atomic Physics, Technische Universität (TU) Berlin, Berlin, Germany, in 2012, and the M.Sc. degree in 2014 from the Institute of Theoretical Physics, TU Berlin, where he is currently working toward the Ph.D. degree. His research interests includes the modeling of nonlinear laser dynamics and stochastic properties of the photon emission in quantum dot lasers.

Benjamin Lingnau received the M.Sc. and Doctoral degrees in physics in 2011 and 2015, respectively, from the Institute of Theoretical Physics, Technische Universität Berlin, Berlin, Germany, where he is currently working as a Postdoctoral Researcher. His research interests include nonlinear laser dynamics, modeling of the optical and dynamic properties of novel semiconductor active materials, and their applications in optoelectronic devices.

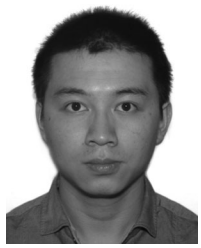

Heming Huang was born in Bengbu, China, in 1989. He received the M.S. degree in material science and engineering from the National Institute of Applied Sciences, Rennes, France, in 2013. He is currently working toward the Ph.D. degree at the Department of Communication and Electronics, Telecom ParisTech, Paris, France. His current research interests include the development of quantum confined devices for optical communications as well as physics and applications of nonlinear dynamics of semiconductor lasers.

Ravi Raghunathan received the Bachelor of Applied Science (Hons.) degree in electrical engineering from the University of Windsor, Windsor, ON, Canada, in 2003, the M.S. degree in electrical engineering (Electrophysics) from the University of Southern California, Los Angeles, CA, USA, in 2006, and the M.S. and Ph.D. degrees in optical science and engineering from the University of New Mexico, Albuquerque, NM, USA, in 2010 and 2013, respectively. From October 2013 to January 2015, he was Postdoctoral Research Associate with the MICS Optoelectronics Research Group, Department of Electrical & Computer Engineering, Virginia Tech, Blacksburg, VA, USA. He received the 2014 Postdoctoral Research Fellowship awarded by the Mairie de Paris as part of the "Research in Paris" program at Télécom Paristech, Paris, France. His current research interests include ultrafast pulse characterization and nonlinear dynamical effects in semiconductor lasers, and nonlinear and quantum optical effects in semiconductor nanostructures.

Kevin Schires received the Diplôme d'Ingénieur degree, specializing in signal processing and telecommunications, from the École Supérieure d'Ingénieurs en Électronique et Électrotechnique, Paris, France, and the Ph.D. degree in semiconductor electronics from the University of Essex, Colchester, U.K. He is currently a Postdoctoral Researcher in the Communications and Electronic Department, Telecom Paristech (former École Nationale Supérieure des Télécommunications), Paris, France, where his research focuses on the study of the dynamics of novel semiconductor laser sources under optical injection and optical feedback.

Philip Poole received the Ph.D. degree in solid-state physics from the Imperial College, London University, London, U.K. After the Ph.D. degree, he pursued a career at the National Research Council Canada, Ottawa, ON, Canada. During this time, he has held many roles such as Researcher, Project Lead, and Group Leader for the Epitaxy group. He is currently a Principle Research Officer in the Information and Communications Technology Portfolio, National Research Council Canada. His research work has covered many areas of III–V semiconductor research including optical spectroscopy, quantum well intermixing, and 20 years of experience in CBE growth of III–V compounds. His research interests include the areas of epitaxial growth of InP-based quantum dot structures for optoelectronic devices that can take advantage of the novel properties of quantum dots, such as multiwavelength and femtosecond modelocked lasers. These are actively being pursued with industrial partners for commercial use. More fundamental studies on the use of selective area epitaxy to control the nucleation site of individual quantum dots for quantum information purposes are also performed. In particular the growth of InP nanowires containing InAs dots with the demonstration of nonclassical optical properties such as photon antibunching and entanglement.

Frédéric Grillot was born in Versailles, France, on August 22, 1974. He received the M.Sc. degree from the University of Dijon, Dijon, France, in 1999, and the Ph.D. degree from the University of Besançon, Besançon, France, in 2003. His doctoral research activities were conducted within the Optical Component Research Department in Alcatel-Lucent working on the effects of the optical feedback in semiconductor lasers, and the impact of this phenomenon has on optical communication systems. From 2003 to 2004, he was with the Institut ds'Electronique Fondamentale, University Paris-Sud, where his research was focused on integrated optics modeling and on Si-based passive devices for optical interconnects. From September 2004 to September 2012, he was with the Institut National des Sciences Appliquées as an Assistant Professor. From 2008 to 2009, he was a Visiting Professor with the University of New-Mexico, Albuquerque, NM, USA, leading research in optoelectronics in the Center for High Technology Materials. Since October 2012, he has been working with Telecom Paristech (alias Ecole Nationale Supsérieure des Télécommunications), Paris, France, where he became an Associate Professor then a Full Professor in January 2017. Since August 2015, he has also been a Research Professor at the University of New-Mexico, Albuquerque, NM, USA. He is the author or coauthor of 77 journal papers, 1 book, 3 book chapters, and more than 170 contributions in international conferences and workshops. His current research interests include advanced quantum confined devices using new materials such as quantum dots and dashes, light emitters based on intersubband transitions, nonlinear dynamics and optical chaos in semiconductor lasers systems as well as microwave and silicon photonics applications including photonic clocks and photonic analog to digital converters. He is an Associate Editor for *Optics Express*, a Senior Member of the SPIE and of the IEEE Photonics Society, as well as a Member of the OSA.

Kathy Lüdge was born in Berlin, Germany, in 1976. She received the Diploma and Dr. rer. nat degrees in physics from the Technische Universität Berlin (TU Berlin), Berlin, Germany, in 2000 and 2003, respectively, and the Habilitation (Venia Legendi) degree from the TU Berlin, in 2011. Since 2016, she has been a Professor of theoretical physics at the TU Berlin and currently on a one year Humboldt Fellowship in the Math Department of the University of Auckland, Auckland, New Zealand. In 2015, she was a Visiting Professor with the Freie Universität Berlin, and from 2011 to 2014, she was a Privatdozentin with the Institute of Theoretical Physics, TU Berlin. From 2001 to 2002, she was a Visiting Scholar with the Department of Material Science, University of Minnesota, Minneapolis, MN, USA. She is an editor of the book entitled *Nonlinear Laser Dynamics—From Quantum Dots to Cryptography* (Volume 5 of Reviews of Nonlinear Dynamics and Complexity) (Wiley, 2011). Her research interests include the modeling of semiconductor quantum-dot lasers, nonlinear laser dynamics, and control with optical feedback.